Aptasensor-enabled quantitative analysis of nano-sized extracellular vesicles by flow cytometry

Jing Du, [*a] Chao Yuan, [a] Weijie Wang, [ce] Zitong Yu, [ae] Rui Hao, [ae] Yi Zhang, [ab] Min Guan,[d] Nan Li[*c] and Hui Yang [*ab]

[a] *Laboratory of Biomedical Microsystems and Nano Devices, Center for Bionic Sensing and Intelligence, Institute of Bio-medical and Health Engineering, Shenzhen Institutes of Advanced Technology, Chinese Academy of Sciences, Shenzhen 518055, CHINA*

[b] *CAS Key Laboratory of Health Informatics, Shenzhen Institutes of Advanced Technology, Chinese Academy of Sciences, Shenzhen 518055, CHINA*

[c] *Center for Synthetic Biology Engineering Research, Shenzhen Institutes of Advanced Technology, Chinese Academy of Sciences, Shenzhen 518055, CHINA*

[d] *Center for Human Tissues and Organs Degeneration, Institute of Biomedicine and Biotechnology, Shenzhen Institutes of Advanced Technology, Chinese Academy of Sciences, Shenzhen 518055, CHINA*

[e] *These authors contribute equally to the work.*

Corresponding Author:

***Phone:** (+) 86-755-64792675.

E-mail: hui.yang@siat.ac.cn (H.Y.); nan.li@siat.ac.cn (N.L.); jing.du@siat.ac.cn (J.D.)

Section 1. Comparison on the different storage method of Apt_CD63

We compared the different storage method of the aptamer. To verify whether the DNA aptamer degrades after long-time freezing at -20°C, Apt_CD63 was dissolved directly in TE buffer (10 mM Tris-HCl pH8.0, 1 mM EDTA) to prepare Sample 1 (Apt 1) at the concentration of 100 mM. In the meantime, Sample 2 (Apt 2) was prepared by dissolving Apt_CD63 in double distilled water (ddH_2O) at 100 mM to make the stock solution, which was stored at -20°C for 3 months before thawing to room temperature. Sample 3 (Apt 3) was made by diluting Sample 2 after thawing to room temperature in PBS buffer to a working concentration. Agarose gel (3%) electrophoresis was then conducted at 120 V for 20 minutes. The commercial Trans DNA Marker I with sizes ranging from 100 bp to 700 bp was used as references. As shown in Supplementary Figure 1, the sizes of all aptamer samples were less than 100 bp. Moreover, there were very limited differences among the three bands of aptamer samples, suggesting that the aptamer was stable in ddH_2O at -20 °C for three months. However, it is better to prepare aptamer solution in PBS freshly, or to dissolve the sample in TE buffer and store at -20 °C for long term usage.

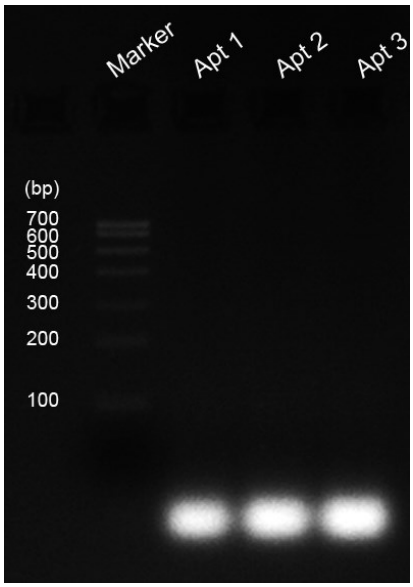

Supplementary Figure 1. Agarose gel electrophoresis analysis of DNA aptamer in water and TE solutions. Apt 1: DNA aptamer in fresh TE buffer; Apt 2: DNA aptamer in fresh ddH_2O; Apt 3: DNA aptamer dissolved in ddH2O and stored for 3 months at -20°C before analysis. 0.5μM DNA aptamer sample was loaded in each lane.

Section 2. Flow cytometry (FCM) calibration with reference beads

Reference silica beads, including 100 nm fluorescent (Excitation/Emission: 485/510 nm) beads, 200

nm, 300 nm, 500 nm beads, were purchased from Kisker Biotech. Beads were diluted to a final concentration of 10 nM in ddH_2O. Importantly, bead solutions in 1.5ml tubes were well mixed by vortex before loaded to FCM, in case microspheres precipitated to form aggregates in solution. First, 100 nm fluorescent beads were utilized to set the thresholds for the FITC-channel on FCM. And the other particles in grey color were background noise (Supplementary Figure 2A). After gating the fluorescent channel (FITC), Violet Side Scatter (VSSC) channel was initiated for determination of beads from the background noise (Supplementary Figure 2B) based on their different surface granularity. Then the VSSC-channel was adopted for detection of beads in solution, histogram and dot plot analysis were utilized for 100 nm fluorescent beads. Two separate peaks or groups were detected, as shown in Supplementary Figure 2C – 2D. Afterwards, the calibrated gate without background noise was applied, thus the signal of beads was clearly represented in the VSSC-channel, as either in a peak (Supplementary Figure 2E) or in a cluster (Supplementary Figure 2F) format. With the same settings of FCM, 200 nm, 300 nm, 500nm beads in solutions were separately loaded to set the maximal detection threshold and appropriate distribution of beads with various diameters. Each sample was detected with a clear peak in the VSSC-channel. Meantime, 4 individual peaks were identified from the mixture of the beads (Supplementary Figure 3A). Moreover, contour plots of these samples also supported that the region of detectable particles were from 100 nm to 500 nm (Supplementary Figure 3B & 4A), which can be distinguished from the background noise. After all these steps, calibrations on light scattering and fluorescent performance of FCM were completed. This provided easy and quick information to the users, whether the current FCM settings was capable for extracellular vesicle (EV) analysis. After bead-based calibration, the EV sample isolated from Bone Marrow-Mesenchymal Stem Cells (BM-MSC) was analyzed on FCM and the size distribution of detected particles in the region from 100 nm to 500 nm was represented in Supplementary Figure 4B. We further used Triton X-100 to lyse the phospholipid membranes of EVs and counted the particles before and after the treatment (Supplementary Figure 4C – 4E). Dramatic decrease of EV count (Supplementary Figure 4F) after detergent lysis demonstrated the successful detection of membraned-encapsulated EVs by FCM.

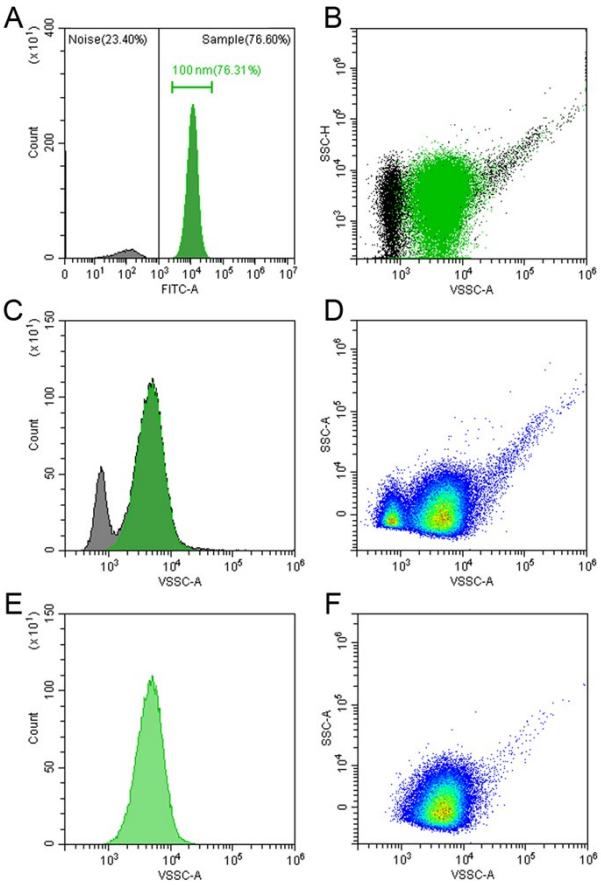

Supplementary Figure 2. Gate setting for FCM using fluorescent beads with diameter of 100 nm. (A) A peak of 100 nm beads (pseudo green) was detected in the FITC-channel; (B) A cluster of 100 nm beads (green) was separated from the background noise (black) in the VSSC-channel. (C) The peak (green in grey background) of 100 nm beads was distinguished from the background noise (grey peak) in the VSSC-channel according to the detectable fluorescent signal in (A); (D) The clusters of the beads (large) and the background noise (small); (E) The single green peak showing the fluorescent beads of 100 nm after gating the VSSC-channel; (F) The distribution pattern of the beads in the VSSC-channel.

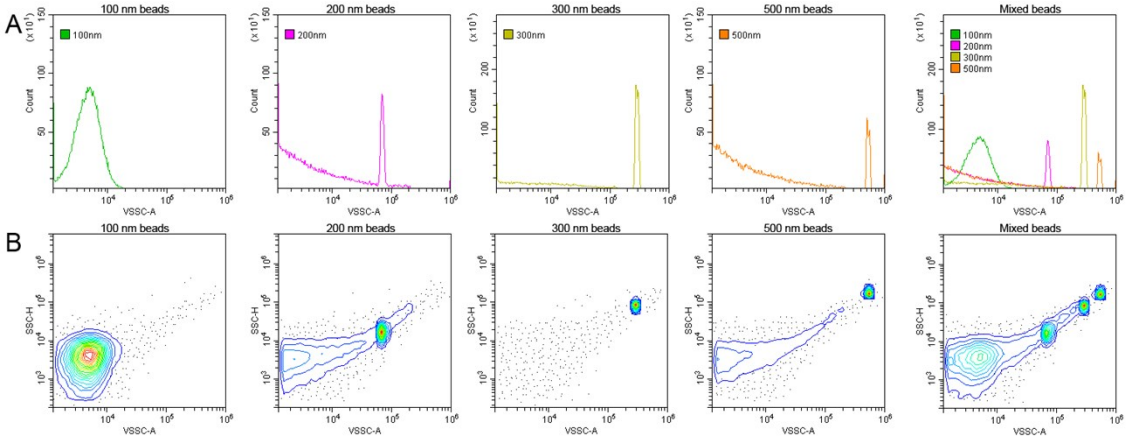

Supplementary Figure 3. FCM calibration using a mixture of nano-sized beads. (A) Surface granularity

measured by VSSC-channel of beads with size of 100 nm (green), 200 nm (pink), 300 nm (yellow), 500 nm (orange) and mixed, respectively; (B) Color-coded regions in contour plot correspond to the results in (A).

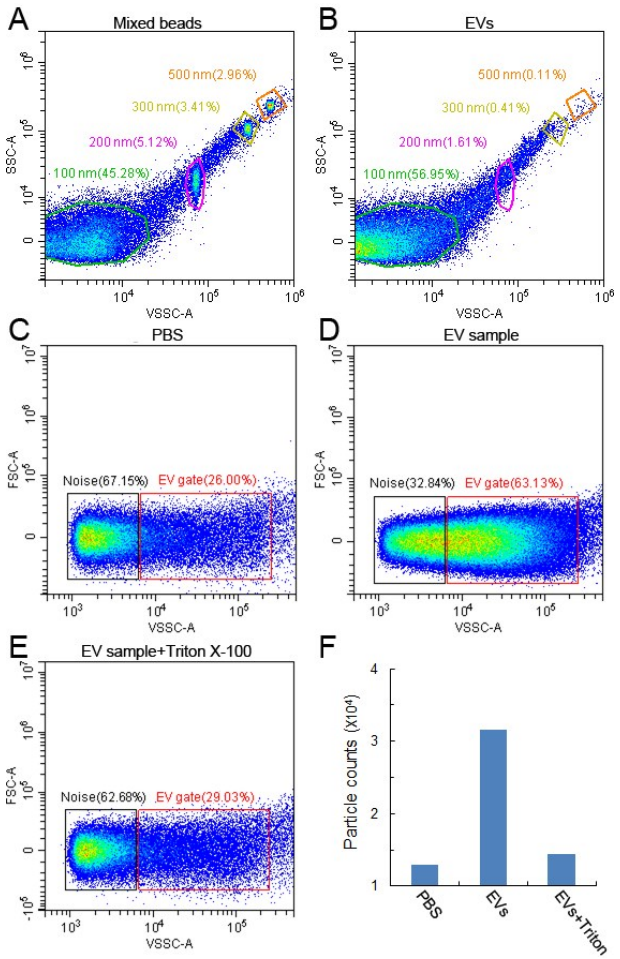

Supplementary Figure 4. Dot plots of EV analysis by the VSSC-channel with mixture of reference beads. (A) Defined size regions using different beads. Green: 100 nm; Pink: 200 nm; Yellow: 300 nm; Orange: 500 nm; (B) Size distribution of EVs derived from BM-MSCs, in the region from 100 nm to 500 nm, using the same setting as mentioned in (A); (C) Scatter plots for Phosphate-buffered saline (PBS); (D) EVs isolated from BM-MSC cell culture supernatant and (E) EVs supplemented with Triton X-100; (F) The number of particles detected in EV gate.

Section 3. Bioinformatic details on the aptamer structure

The aptamer for human CD63 protein (Apt_CD63) was screened and selected from DNA combinatorial library through Systematic Evolution of Ligands by Exponential enrichment (SELEX) [1]. This single-stranded DNA (Apt_CD63) consisting of 32-base nucleotides was firstly reported for exosome and EV detection by Revzin's group [2]. It's known that aptamer selectively binds to a specific

target, determined by its tertiary structure rather than the primary sequence. Although Apt_CD63 has shown high affinity to CD63, the bioinformatic details on its tertiary structure remains unclear. Here we use RNAComposer software [3] to model its three-dimensional (3D) structure. First, RNAstructure software [4] was utilized for secondary structure prediction of this single-strand nucleic acid chain (Supplementary Figure 5A). Then, the secondary structure in required format was put into RNAComposer for the prediction of its tertiary structure (Supplementary Figure 5B). The Apt_CD63 was synthesized based on the reported sequences [2]. Moreover, the mass spectrum assessment was performed for quality control (Supplementary Figure 6).

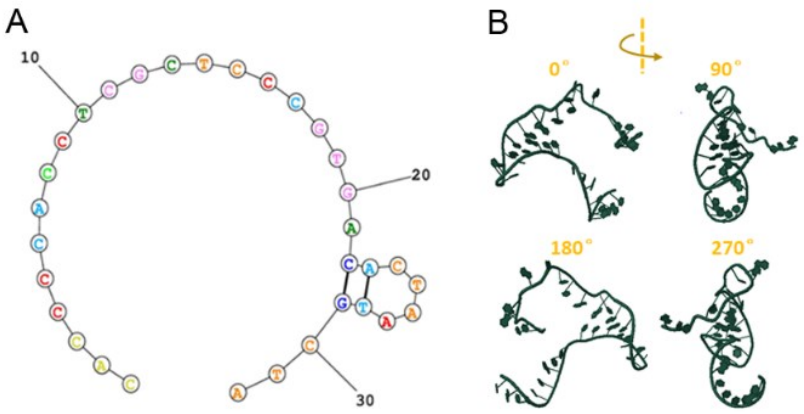

Supplementary Figure 5. Bio-information analysis of Apt_CD63. (A) Secondary structure of Apt_CD63; (B) Tertiary structure of Apt_CD63.

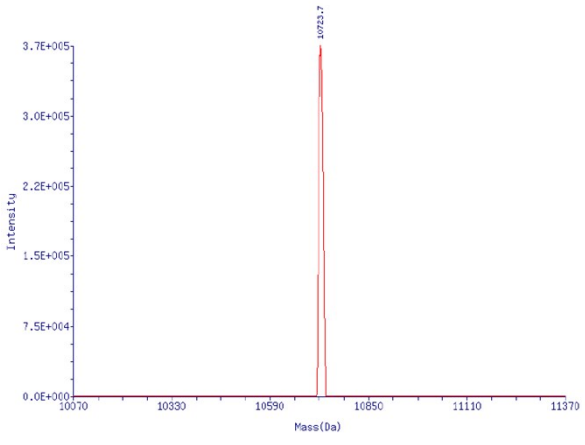

Supplementary Figure 6. Mass spectrometry of the synthetic Apt_CD63.

Section 4. Optimization on the Apt_CD63 reaction condition for EVs analysis on FCM

Previous works successfully detected EVs using Apt_CD63 in PBS [3] and TBE [4] buffer without blocking agents. In this work, we tested blocking agents in the binding experiment. 1% BSA is usually used as the blocking agent in immunoassays for CD63 proteins on EVs [5]. Under this condition, the concentration of BSA in the solution is ~ 9×10^{19} molecules/L. Considering the concentration of EVs in the sample is ~ 1×10^{12} particles/L, therefore, ~ 9×10^{7} BSA molecules are used to block one EV, which is quite adequate. We also tested ssDNA as the blocking agent. To reach the equal molecular concentration of ssDNA per EV as BSA, the concentration of ssDNA is calculated as 150 μM.

In the binding experiments, EVs were firstly incubated with 150 μM ssDNA (the same nucleic acid sequence as mutated Apt_CD63 without fluorescein) or 1% (w/v) bovine serum albumin (BSA) in PBS, respectively, for 1 hour. Then, 80 nM Apt_CD63 was applied to the sample and kept at room temperature for 15min until FCM analysis. The EVs labeled by fluorescent Apt_CD63 without using the blocking agents were defined as the control group, the relative labeling efficiency of Apt_CD63 labeled EVs is ~ 50% (Supplementary Figure 7A). The sample blocked by 150 μM ssDNA shows an increased labeling efficiency of ~ 54% (Supplementary Figure 7B). The ssDNA in solution may block the EVs membrane, but the ones on the membrane can also induce specific binding to the fluorescent Apt_CD63 afterwards, generating a higher detection signal and showing that ssDNA is not suitable as the blocking agent. On the other hand, the sample blocked by 1% BSA shows a suppression on the labeling efficiency of EVs (Supplementary Figure 7C – 7D). BSA not only blocks the excess binding sites on the EVs membrane, but also prevents the interaction between Apt_CD63 and membrane protein CD63 by occupying the interaction sites, resulting in a reduction of the detected events on FCM. Moreover, the BSA molecules in the sample can interact with the CFSE dye, therefore introducing an overvaluation on the protein components in the sample, generating errors on the dual-staining results of FCM analysis. To summarize, using ssDNA or BSA to block the sample introduces uncertain factors into the evaluation system and results in variations on the dual-staining efficiency for FCM analysis. We therefore chose PBS buffer without blocking agents for dual-staining procedure on EVs analysis by FCM.

To further optimize the aptamer-based labeling procedure, Apt_CD63 solutions with a series of concentrations from 0.01 nM to 100 nM were prepared and then analyzed by the FCM. The samples were analyzed by the Forward Scatter (FSC)-channel, the overlay peaks (Supplementary Figure 8A) suggested

that the size of particles in solution was not affected by the Apt_CD63. Similar phenomenon was found in the Side Scatter (SSC)-channel (Supplementary Figure 8B). To avoid missing details of particles sizing from 100 nm to 150 nm [5], the VSSC analysis was also applied to all the samples. The result showed limited difference among overlay peaks (Supplementary Figure 8C), indicating that Apt_CD63 was very uniform in water with final concentration of no more than 100 nM. Further data analysis on the Apt_CD63 solutions showed that there was no obvious difference among samples at concentrations of no more than 1 nM (Supplementary Figure 9A – 9B). However, when the concentration increased to 80 nM, there was a dramatic difference on surface granularity comparing to that of 1 nM on the VSSC channel (Supplementary Figure 9C – 9D). The Apt_CD63 solutions with concentrations higher than 10 nM were used thereafter, and applied to EVs derived from BM-MSCs. As shown in Supplementary Figure 10A, the peaks of the fluorescent channel shifted gradually towards higher intensities when the concentration of the solution increased. When the sample is of 100 nM in concentration, the result showed a dramatic difference than the others, and the similar pattern was also found in the CFSE channel when dual-staining was applied to the EVs derived from BM-MSCs, neural stem cells (NSCs) and epidermal cells (Supplementary Figure 10B-D). On the other side, light scattering channels were also checked in the same manner. The perfect overlay suggested that Apt_CD63 showed no impact on the size distribution of EVs in the FSC-channel (Supplementary Figure 11A). Furthermore, slight difference in the SSC-channel was obtained (Supplementary Figure 11B), and big difference shown in Supplementary Figure 11C indicated it was applicable to distinguish samples by the VSSC-channel. Therefore, in summary, 80 nM was the optimal concentration of Apt_CD63 to label EVs for further analysis by both fluorescent and VSSC channels.

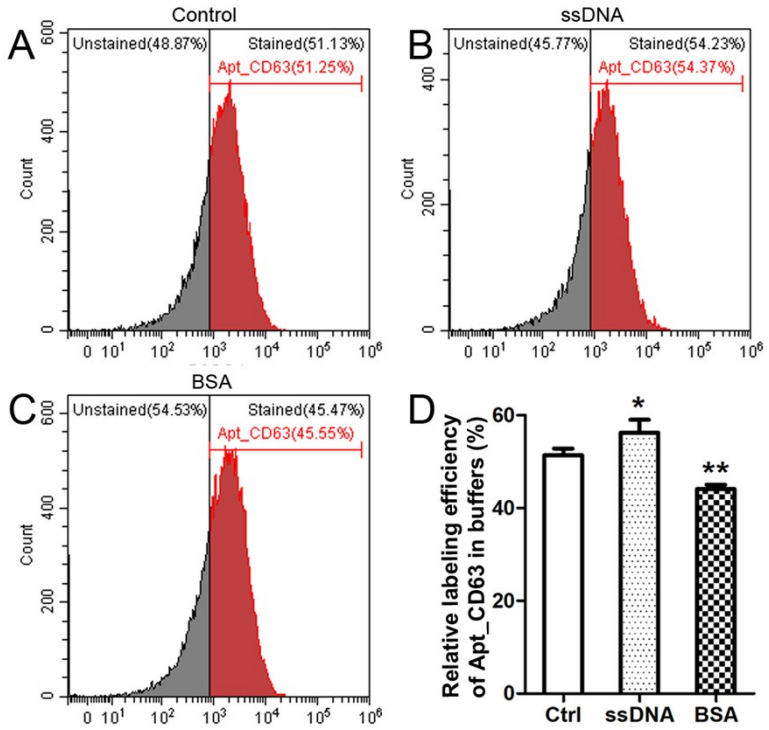

Supplementary Figure 7. Comparation on the labeling efficiency of EVs using different methods. Plots of EVs stained by fluorescent Apt_CD63 at a low concentration of 80nM in (A) PBS buffer, (B) PBS buffer supplemented with 150 μM ssDNA as the blocking agent, and (C) PBS buffer supplemented with 1% BSA as the blocking agent, respectively. (D) Relative labeling efficiency of EVs reacting with Apt_CD63 in buffer (A)-(C). Data are mean values ± SE, with three biological repeats for each sample. Asterisks indicate significant differences (Student's t-test, *, P< 0.1; **, P< 0.01).

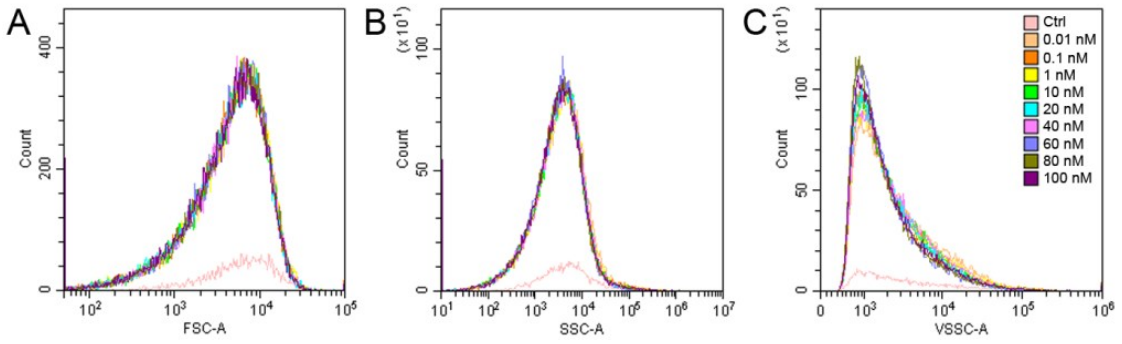

Supplementary Figure 8. Overlay histogram analysis of size and surface granularity of Apt_CD63 at various concentrations. (A) FSC measurement showed non-discrimination of Apt_CD63 by size; (B) SSC measurement showed similar surface granularity; (C) VSSC measurement presented limited difference on surface granularity of Apt_CD63 in water at different concentrations, detected by enhanced light-scatter sensitivity.

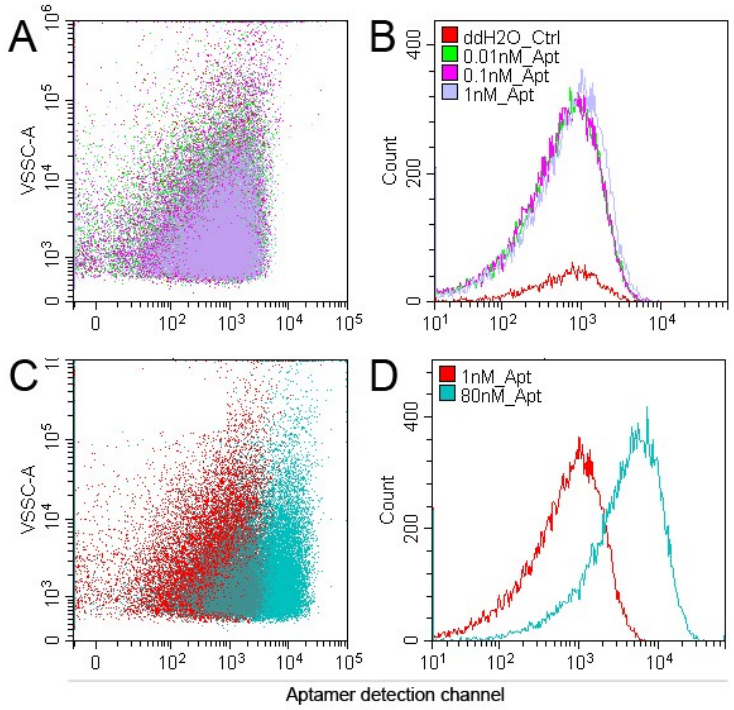

Supplementary Figure 9. Detection limitation and efficiency of Apt_CD63 in the fluorescent channel. (A) Overlay dot plot and (B) histogram analysis of Apt_CD63 at concentrations of no more than 1 nM, comparing to the control (water); (C) Dense dots in triangle shape showed great discrimination between Apt_CD63 sample at concentration of 1 nM (red color) and 80 nM (blue color); (D) Overlay histogram analysis of Apt_CD63 showed dramatic differences at indicated concentrations.

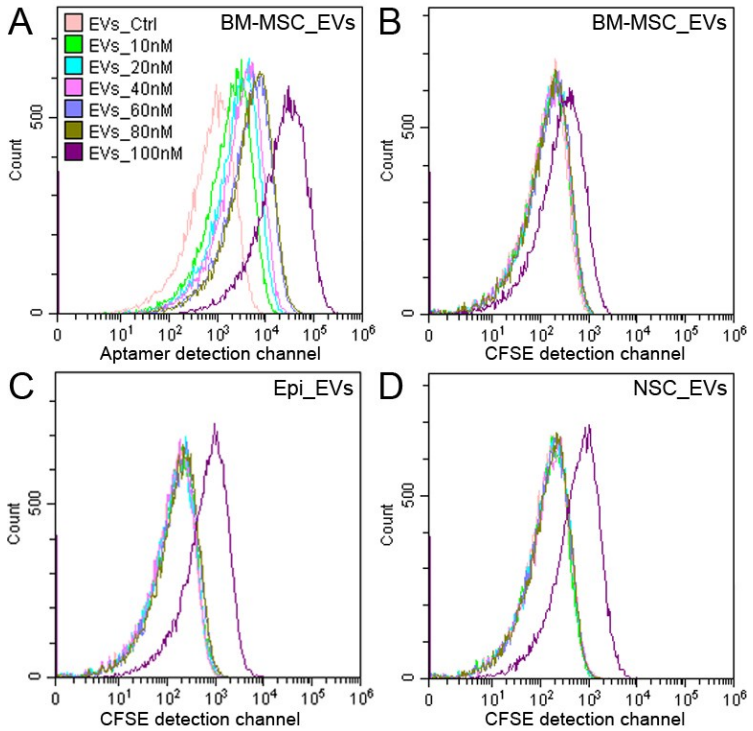

Supplementary Figure 10. Dual-staining method-based fluorescent analysis of EVs with Apt_CD63 in a concentration-dependent manner. The peak in purple color represented an obvious shift from the rest in the aptamer channel when 100 nM Apt_CD63 was applied to (A) BM-MSC derived EVs, (B) BM-MSC derived EVs, (C) epidermal cells (Epi)-derived EVs and (D) neural stem cells (NSC)-derived EVs. The results were obtained from the CFSE channel after the dual-staining.

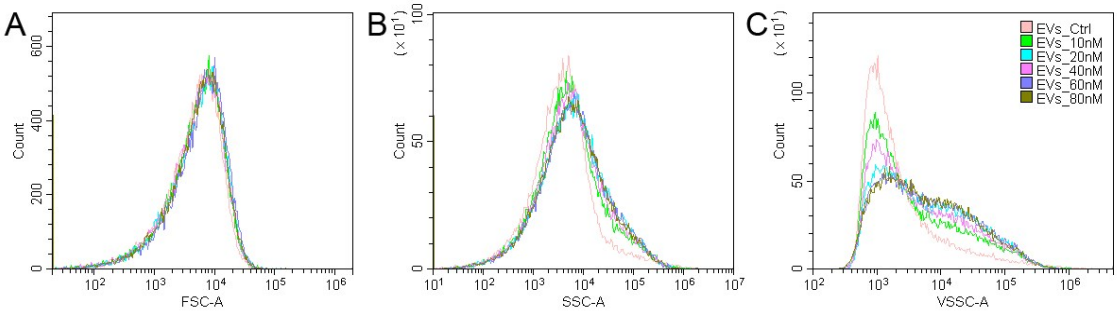

Supplementary Figure 11. Overlay histogram analysis of size and surface granularity of EVs with and without Apt_CD63. (A) The precise overlay of EV samples with and without Apt_CD63 at varying concentrations in the FSC-channel; (B) SSC measurement showed similar surface granularity of EVs after being supplemented with Apt_CD63; (C) Dramatic difference of EVs in the presence of varying amount of Apt_CD63, detected by the VSSC-channel due to its enhanced light-scatter sensitivity.

Section 5. Optimization of the fluorescent detection channels

After 80 nM was chosen as the optimal concentration, single-staining with either Apt_CD63 or CFSE dye was utilized to set the threshold for fluorescent detection. CFSE dye (Cat# 65-0850-84, eBioscience, Thermo Fisher) is reported with excitation peak at 492 nm and emission peak at 517 nm. It was excited by the 488 nm laser, and emission spectrum between 505 nm and 545 nm was collected by the FITC channel on the FCM. While Cy5.5 conjugated with Apt_CD63 is reported with excitation peak at 565 nm and emission peak at 693 nm, which was excited by the 561 nm laser and emission spectrum between 665 nm and 715 nm was collected by the PerCP PC5 channel on the FCM. There is no interference between these two channels in principle. And the dual-stained sample using CFSE dye followed by Apt_CD63 was also monitored under the same setting. It was found that Apt_CD63 didn't affect the fluorescent detection of CFSE (Supplementary Figure 12A), and similar effect of CFSE on the aptamer channel was also observed (Supplementary Figure 12B). Those results suggested that 488 nm laser with 525±20 nm emission filter is optimal setting for CFSE detection and 561 nm laser with 690 ± 25 nm emission filter is optimal setting for the detection of Apt_CD65 linked with Cy5.5 on the FCM.

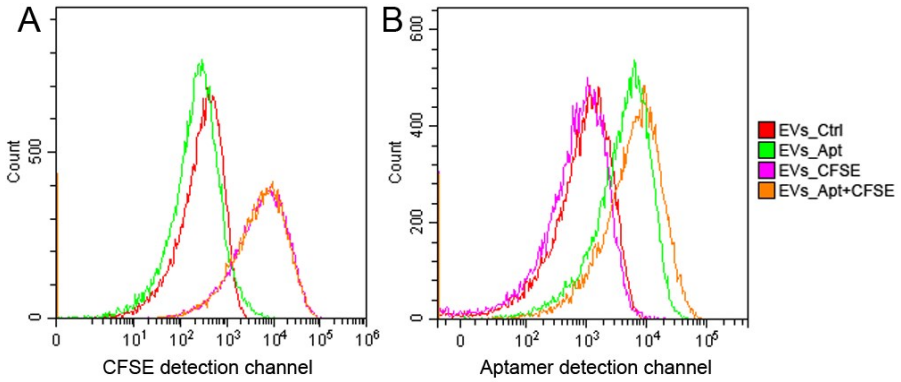

Supplementary Figure 12. Fluorescent detection of EVs by single- and dual-staining. (A)Overlay histogram of EVs showed a dramatic difference with and without CFSE staining in CFSE-detection channel; (B) EV samples with dual staining and Apt_CD63 staining represented similar pattern in fluorescent aptamer detection channel.

Section 6. Comparison on different cell culturing media

To test whether the choice of FBS serum influenced the final production and detection of EVs, the cells from human cornea epithelial cell-2 (HCE-2) cell line were cultured in normal FBS and exosome-depleted FBS for 2 days, respectively. The supernatant of two culturing media were collected separately for EV isolation and FCM analysis. As shown in Supplementary Figure 13, there were 25.88% dual-stained particles obtained from exosome-depleted FBS, whilst 24.83% from normal FBS medium, indicating that HCE-2 secretes equivalent EV amount in the two types of culturing medium. Thus, EVs in FBS serum contribute more to supply extracellular matrix for cell growth, but not to the total amount of EVs.

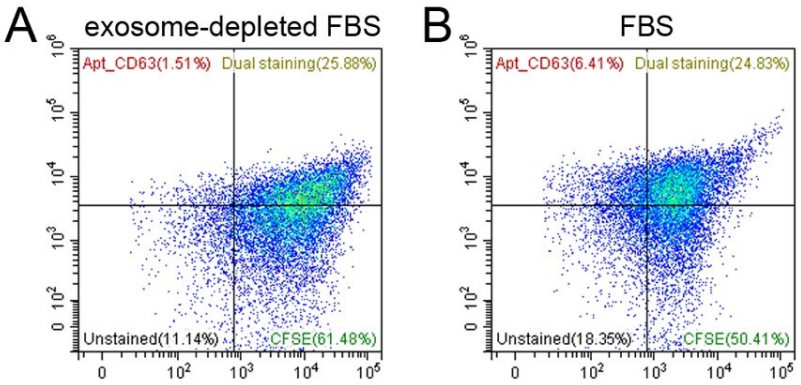

Supplementary Figure 13. Apt_CD63-based dual staining analysis of EVs derived from HCE-2 cultured in (A) exosome-depleted FBS and (B) normal FBS serum.

Section 7. Comparison of Apt_CD63 and anti-CD63 antibody

As a comparison, PE-eFluor®610 (excitation peak: 566 nm, emission peak: 610 nm) conjugated anti-CD63 monoclonal antibody (Cat#61-0639-42, Invitrogen) was used to label EVs derived from different cell lines. The PE-eFluor®610 dye was excited by the 561 nm laser and emission spectrum between 665 nm and 715 nm was collected by the PerCP PC5 channel on the FCM. The result shows that the labeling efficiency with anti-CD63 antibody was less than 10% when it's incubated with EVs for 15 min, compared to that with Apt_CD63 of more than 50%. As shown in Supplementary Figure 14 and 15, when the EVs were incubated with anti-CD63 antibody for 4 hours, the labeling efficiency is comparable to those with Apt_CD63 for 15 min, indicating the characteristics of fast response and high efficiency of Apt_CD63. Moreover, by comparing the labeling behavior with the aptamer and the antibody, the variations on the relative labeling efficiency of Apt_CD63 on different cell lines can be neglected, suggesting that aptamer shows stable performance when applied to different samples.

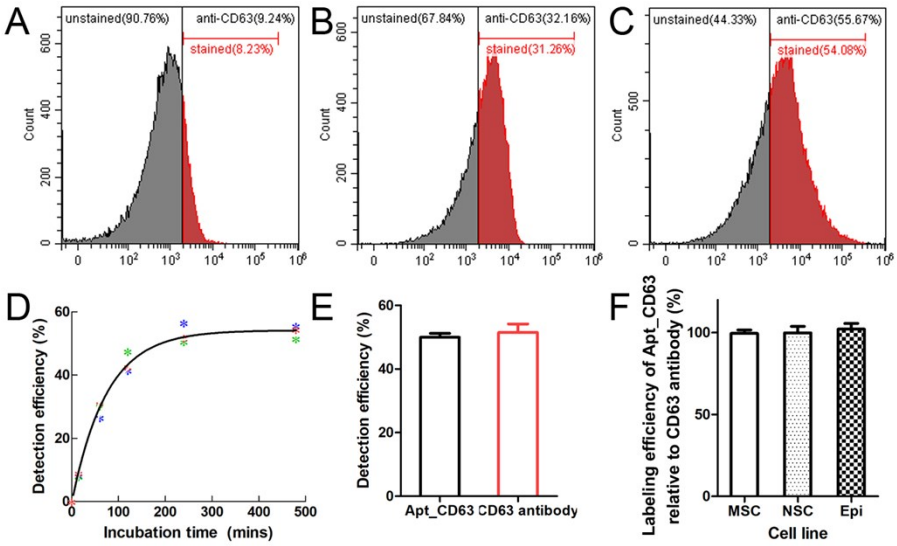

Supplementary Figure 14. Cytometric analysis of EVs with the anti-CD63 antibody. (A-C) A cluster of stained particles detected in fluorescent channel after MSC-derived EVs reacting with anti-CD63 antibody for 15 mins (A), 1h (B), and 4h (C), respectively; (D) labeling efficiency of MSC-EVs labeled by anti-CD63 antibody with different incubation time. Asterisks indicate three biological repeats at each time point; (E) Labeling efficiency of MSC-derived EVs reacting with Apt_CD63 and anti-CD63 antibody; (F) Relative labeling efficiency of Apt_CD63 and anti-CD63 on MSC-EVs, NSC-EVs and Epi-EVs. Relative labeling efficiency = Labeling efficiency of Apt_CD63/Labeling efficiency of anti-CD63 antibody.

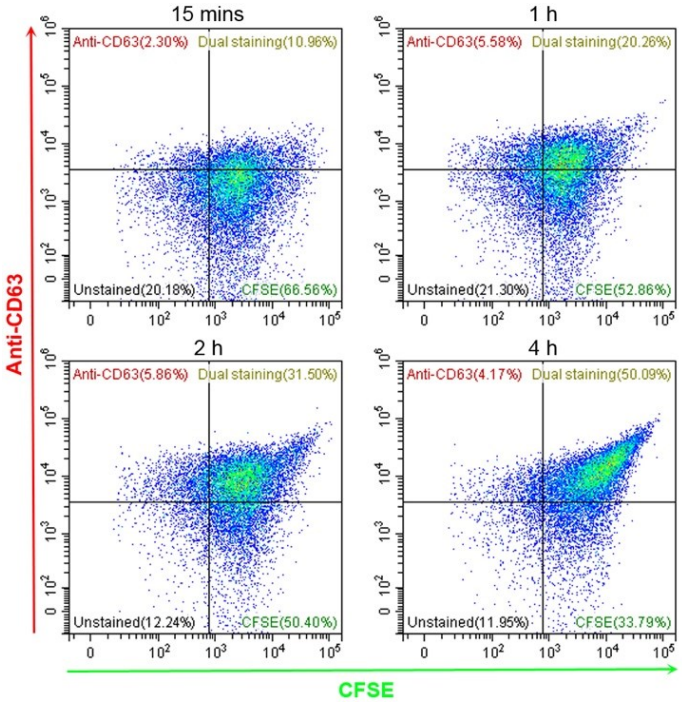

Supplementary Figure 15. Multiplexed analysis of EVs using anti-CD63-based dual staining method. MSC-derived EVs were stained with CFSE and then incubated with anti-CD63 for 15minutes, 1h, 2h and 4h, respectively.

Furthermore, to evaluate the specificity of Apt_CD63, dual-staining of EVs using Apt_CD63 and anti-CD63 antibody was performed. MSC-derived EVs were incubated with Apt_CD63 (80 nM) in 1% PBS-BSA (1% w/v BSA in 1× PBS) first at room temperature for 15 minutes in the dark, followed by incubation with anti-CD63 monoclonal antibody for 4 hours at 37 ºC in the dark. Obtained from the FCM analysis, the double labeled EVs reached 34.71% in the 4th quadrant, considering the Apt_CD63 labeled EVs takes 59.2% among the whole detected population (Supplementary Figure 16A), therefore, this result indicates that 58.6% of Apt_CD63 labeled EVs was also recognized by the antibody. Moreover, when the EVs were labeled by the anti-CD63 antibody first and then the aptamer, the double labeled EVs are 25.69% in the sample (Supplementary Figure 16B), suggesting that 46.5% of the antibody labeled EVs was co-labeled by the apt_CD63. The higher proportion of the co-labeled EVs when applying the aptamer first presents that the affinity of the antibody to the membrane protein is a bit higher than that of the aptamer. It should be noted that the reaction of EVs with the antibody takes 4 hours, comparing to only 15 minutes with the aptamer, indicating the fast response of the aptamer without compromising too much on the efficiency and specificity of the labeling method. Moreover, in the manuscript, Apt_CD63-based labeling

efficiency was over 50% from FCM analysis, and it dropped to 0.46% when using the mutated aptamers, suggesting that the detected unspecific binding is very low and well controlled.

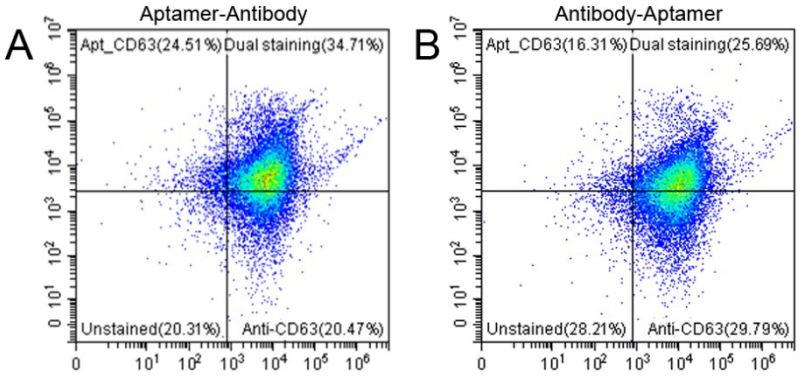

Supplementary Figure 16. Multiplexed analysis of EVs using apt_CD63 and antibody-based dual staining method. (A) The EVs were labeled by Apt_CD63 and then antibody. (B) The EVs were labeled by anti-CD63 antibody and then Apt_CD63.

Section 8. Comparison of Apt_CD63 and a mutated aptamer

Aptamers are short, single-stranded oligonucleotides (DNA or RNA), evolved from random oligonucleotide libraries by a process called Systematic Evolution of Ligands by Exponential Enrichment (SELEX) [6]. Aptamers act as ligands with specific and high binding affinity by folding into tertiary structures [7]. Here, the Apt_CD63 binds to CD63 protein efficiently and specifically in PBS buffer. And complementary DNA sequences of Apt_CD63 was used to stop further binding reaction. It's reported that the DNA sequences can open the aptamer structure, thus to stop the interaction between Apt_CD63 and CD63 protein on EV membrane successfully [8]. The non-labeled MSC-derived EV sample was recorded as control (ctrl) and analyzed in fluorescent channel by flow cytometry (Supplementary Figure 17A). A shuffled fluorescent Apt_CD63 (shuffled Apt), thrombin aptamer [9] and streptavidin aptamer [10] with corresponding sequences of ACACTCCAACTCGCTTCCACGTCGGACTCACC-Cy5.5, GGTTGGTGTGGTTGG-Cy5.5 and TATAACGCCCGTGTTGCTCGGTTAT-Cy5.5 were purchased from GENEWIZ Inc. and purified by HPLC. Mass spectrum assessment was also performed for quality control. According to the equilibrium condition for reaction between Apt_CD63 and EVs in the previous publication [11], BM-MSC derived EVs were incubated with the aforementioned three kinds of aptamers for 15mins before FCM analysis. The Apt_CD63 and the three kinds of aptamers were firstly analyzed on FCM at the concentration of 80 nM, and then those aptamers were separately applied to the EV samples

derived from MSCs for FCM analysis. Without BM-MSC derived EVs, the percentage of fluorescent background for Apt_CD63 aptamer is ~12%, comparatively to that of ~16% for shuffled Apt_CD63 aptamer (Figure 1 A-B). The labeling efficiency of EVs using Apt_CD63 is ~50%, while the labeling efficiency is dramatic significantly reduced in shuffled aptamer labeled EV sample (Figure 1 C-E). Moreover, another two negative control (thrombin aptamer, and streptavidin aptamer) were tested in the same condition. The results showed that there was detectable relative labeling efficiency using non-specific aptamers, suggesting that non-specific binding is ubiquitous. More importantly, the relative labeling efficiency of Apt_CD63 is much higher than the rest aptamers. Statistical test shows significant difference (Figure 1 F). Therefore, Apt_CD63 aptamer represents high affinity towards EV sample than the other aptamers.

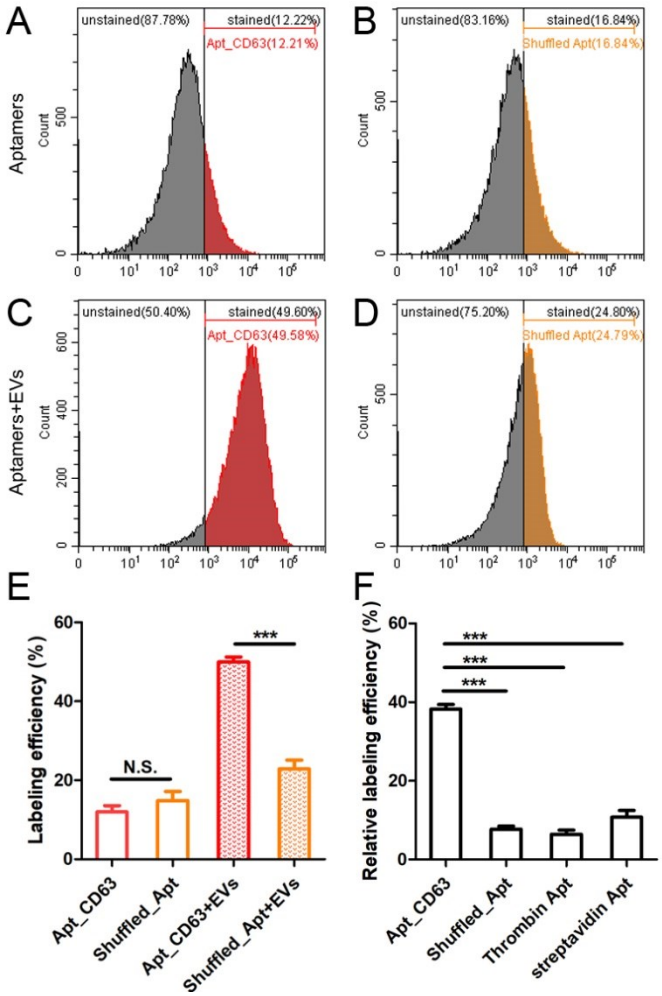

Supplementary Figure 17. A plot of FCM analysis on MSC-derived EVs labeled using different kinds of aptamers. (A-B) A cluster of fluorescent background detected in fluorescent channel with Apt_CD63 (A) and shuffled aptamer (B); (C-D) A peak of MSC-derived EVs interacting with Apt_CD63 (C) and shuffled aptamer (D) in the same fluorescent channel; (E) Percentage of labeling efficiency obtained from samples reacting with

and without Apt_CD63 or shuffled aptamer; (F) Percentage of relative labeling efficiency of EVs using Apt_CD63, shuffled aptamer, thrombin aptamer, and streptavidin aptamer, respectively. Data are mean values ± SE, with three biological repeats for each sample. Asterisks indicate significant differences (Student's t-test, ***, P< 0.001).

Reference:

[1]. J. Yan, H. Xiong, S. Cai, N. Wen, Q. He, Y. Liu, D. Peng, Z. Liu, Advances in aptamer screening technologies, *Talanta* **200** (2019) 124-144.

[2]. Q. Zhou, A. Rahimian, K. Son, D.-S. Shin, T. Patel, A. Revzin, Development of an aptasensor for electrochemical detection of exosomes, *Methods* **97** (2016) 88-93.

[3]. Z. Wang, S. Zong, Y. Wang, N. Li, L. Li, J. Lu, Z. Wang, B. Chen, Y. Cui, Development of an aptasensor for electrochemical detection of exosomes, *Nanoscale* **10** (2018) 9053-9062.

[4]. X. Chen, J. Lan, Y. Liu, L. Li, L. Yan, Y. Xia, F. Wu, C. Li, S. Li, J. Chen, A paper-supported aptasensor based on upconversion luminescence resonance energy transfer for the accessible determination of exosomes, *Biosens. Bioelectron.***102** (2018) 582-588.

[5]. C.S. Carmen, S. Henar, J.A. Ricardo, L.E. Estefanía, M.P. Luis, Y.M. María, V.G. Mar, High sensitivity detection of extracellular vesicles immune-captured from urine by conventional flow cytometry, *Sci. Rep.* **9** (2019) 2042.

[6]. M. Biesiada, K.J. Purzycka, M. Szachniuk, J. Blazewicz, R. W. Adamiak, Automated RNA 3D structure prediction with RNAcomposer, *Methods Mol. Biol.* **1490** (2016) 199-215.

[7]. J.S. Reuter, D.H. Mathews, RNAstructure: software for RNA secondary structure prediction and analysis, *BMC Bioinformatics* **11** (2010) 129.

[8]. G.C. Brittain IV., Y.Q. Chen, E. Martinez, V.A. Tang, T.M. Renner, M.-A. Langlois, S. Gulnik, A novel semiconductor-based flow cytometer with enhanced light-scatter sensitivity for the analysis of biological nanoparticles, *Sci. Rep.* **9** (2019) 16039.

[9]. B. Deng, Y. Lin, C. Wang, F. Lin, Z. Wang, H. Zhang, X. Li, X. Le, Aptamer binding assays for proteins: the thrombin example--a review, *Anal. Chim. Acta* **837** (2014) 1-15.

[10]. C. Wang, G. Yang, Z. Luo, H. Ding, In vitro selection of high-affinity DNA aptamers for streptavidin, *Acta Biochim. Biophys. Sin.* **41** (2009) 335-340.

[11]. K. Zhang, Y. Yue, S.X. Wu, W. Liu, J.J. Shi, Z. Zhang, Rapid capture and nondestructive release of extracellular vesicles using aptamer-based magnetic isolation, *ACS Sensors* **4** (2019) 1245-1251.